



Optics Letters

16.9 W average power from a diode-pumped picosecond Yb:YAG laser with a large-size rectangular core crystalline waveguide

GUOTAI LI,¹ SHUAI LI,¹ KAILUN ZHANG,¹ ZHANDA ZHU,^{1,2,3,4} YONGLING HUI,^{1,2,3,4} HONG LEI,^{1,2,3,4,5} AND QIANG LI^{1,2,3,4,6}

¹Institute of Laser Engineering, Faculty of Materials and Manufacturing, Beijing University of Technology, Beijing 100124, China

²Key Laboratory of Trans-scale Laser Manufacturing Technology, Ministry of Education, Beijing 100124, China

³Beijing Engineering Research Center of Laser Technology, Beijing 100124, China

⁴Beijing Higher Institution Engineering Research Center of Advanced Laser Manufacturing, Beijing 100124, China

⁵e-mail: leihong@bjut.edu.cn

⁶e-mail: ncltlq@bjut.edu.cn

Received 5 December 2021; revised 26 December 2021; accepted 27 December 2021; posted 5 January 2022; published 8 February 2022

We demonstrate a high-power all-solid-state picosecond laser based on a passive mode-locking laser with a large-size rectangular core crystalline waveguide and a semiconductor saturable-absorber mirror. An average power of 16.9 W is achieved with a 1.96 ps duration and a 31.74 MHz repetition frequency. This is the first demonstration of a mode-locked laser with a large-size rectangular core crystalline waveguide to our knowledge. © 2022 Optica Publishing Group

<https://doi.org/10.1364/OL.449687>

Ultrashort pulse laser sources with high average power are an indispensable tool for many industrial and scientific applications, including laser precision micromachining and cutting, high-harmonic generation, and attosecond science [1–3]. At present, the main way to obtain high-power ultra-short pulses is through various amplification systems [4]. However, amplified spontaneous emission (ASE) is added by amplifier chains [5]. Therefore, the development of an ultra-short pulse oscillator with a simple structure, high average power, and low-noise properties would be significant.

Traditional solid-state laser oscillators use block crystals as a gain medium. Heat accumulation in the crystals produces thermal distortions, and it is difficult to maintain a fundamental transverse mode of constant size at high power. In order to improve the thermal effect on the gain medium, researchers have proposed an optical fiber [6], photonic crystal fiber [7], thin disk [8], slab [9], and crystal waveguide [10]. Crystal waveguide lasers are considered to have the potential to achieve high power and near diffraction-limited laser output due to their characteristics of a limiting laser mode, high one-way gain, a large surface-volume ratio, high thermal conductivity, and a high nonlinear threshold. Yttrium aluminum garnet (YAG) crystal waveguides have been fabricated by many different techniques, including pulsed laser deposition (PLD), ion implantation, laser inscription, and liquid-phase epitaxy (LPE) [11]. By taking full advantage of the high-gain characteristics of the waveguide structure, the lasers can be integrated to achieve multi-GHz

repetition rate mode-locking operation [12]. Due to the small core size (usually 10 μm) of a single-transverse-mode crystalline waveguide, it is difficult to achieve a high average power output. An alternative crystal waveguide preparation method is the diffusion bonding technique. The advantage of this method is that crystal waveguides with low loss and large-mode-area structures can be fabricated. In 2014, Mu *et al.* [13] fabricated a double-clad Yb:YAG crystal square waveguide with a core diameter of 40 $\mu\text{m} \times 40 \mu\text{m}$ by direct bonding, and realized continuous-wave (CW) laser output of the fundamental transverse mode. In 2019, near-diffraction-limited laser CW output was demonstrated using a large-size core crystalline waveguide (320 $\mu\text{m} \times 400 \mu\text{m}$) laser based on refractive index matching of the cladding with the core and core mode competition [14]. The average output power and the output pulse energy of a crystalline waveguide laser can be improved by increasing the diameter of the core while maintaining the high beam quality. A large-size rectangular core crystalline waveguide provides a new scheme for high-power mode-locked lasers, but, to date, no large-size rectangular core crystalline waveguide mode-locking laser has been demonstrated.

In this Letter, we report on a Yb:YAG large-size rectangular core crystalline waveguide soliton-mode-locked laser that generates an average power of 16.9 W and has a repetition frequency of 31.74 MHz for 1.96 ps pulses. The main limiting factors and solutions for achieving high-power output of large core crystal square-waveguide mode-locking lasers are studied. To the best of our knowledge, this is the first demonstration of a large-size rectangular core crystalline waveguide mode-locking laser.

Yb:YAG crystal is an attractive gain medium for high-power ultra-short pulse lasers due to its long fluorescent lifetime, high thermal conductivity, excellent thermo-mechanical properties, and broad absorption band and gain bandwidth. However, its small emission cross section is not conducive to the realization of continuous-wave mode locking (CWML). In a mode-locking laser, the semiconductor saturable-absorber mirror (SESAM) needed for mode locking introduces a tendency for the laser to present Q-switching instabilities. This problem is particularly

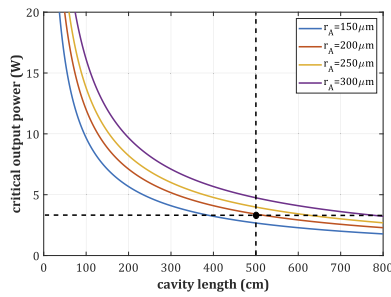


Fig. 1. The influences of the cavity length and spot size on the threshold for CWML.

severe for a Yb:YAG large-size rectangular core crystalline waveguide mode-locked laser that has a large spot size in the gain medium and a low laser emission cross section. We succeeded in suppressing Q-switching mode locking (QML) with a combination of methods. First, an output coupler with a comparatively low transmission was used to increase the beam power density in the cavity. Second, we designed a laser cavity with a low repetition rate. Third, we used a SESAM with a relatively small modulation depth and saturation fluence to reduce the pulse energy threshold of CWML. Fourth, we used Gires–Tournois interferometer (GTI) mirrors to compensate for the positive dispersion and self-phase modulation in the cavity, and to obtain a stable mode-locking signal.

In order to suppress QML, we analyzed the influences of cavity length and spot size (on the SESAM) on the threshold of CWML [15] (Fig. 1).

We determined the cavity length and spot size on the SESAM by considering the following factors: (1) the energy density on the SESAM is 3–5 times greater than the saturation fluence of SESAM, which is less than the damage threshold and therefore stops the Q-switched pulses from damaging the SESAM by, and (2) the CWML status output power threshold is smaller than the maximum CW operation output power. According to the calculation results, the cavity length is set to 5 m, the corresponding repetition frequency is 30 MHz, the spot radius on the SESAM is 200 μm , and the theoretical CWML threshold output power is 3.1 W. The SESAM is controlled by a water-cooled copper block to ensure steady laser operation.

The large-size rectangular core crystalline waveguide used in the experiment was fabricated by the diffusion bonding technique. The crystal bonding processes included precision polishing, optical contacting, and heat treatment. Its structure consists of three parts (Fig. 2). The core layer is 1.0 at.% Yb:YAG with a cross-section size of 320 $\mu\text{m} \times 400 \mu\text{m}$. The length and width of the core layer are different as this allows us to study the maximum core layer diameter that can achieve

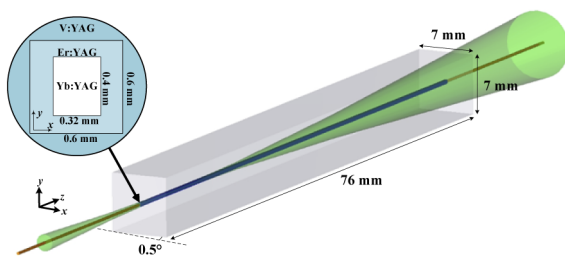


Fig. 2. Structure of the crystal waveguide (inset: schematic diagram of an end face).

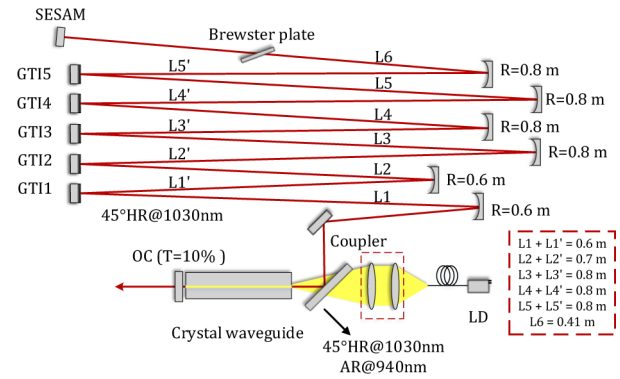


Fig. 3. Experimental setup of the large-size rectangular core crystalline waveguide mode-locked laser.

TEM00 mode operation. The cladding is 0.5 at.% Er:YAG with a cross-section size of 600 $\mu\text{m} \times 600 \mu\text{m}$. The refractive index difference between the Yb:YAG and Er:YAG was measured to be only 4×10^{-6} (to an accuracy of approximately 10^{-7}) by the interferometric measurement method [16]. 4.0 at.% V:YAG was chosen for the outside of the cladding material; large dimensions (7 mm \times 7 mm) were selected in order to absorb ASE and improve the mechanical strength of this waveguide [17]. A high-transmittance coating layer and 0.5° angles of both end surfaces are used to suppress the parasitic oscillation resulting from the residual reflection at the end surfaces and to increase the stability of the mode locking. The length of the crystalline waveguide is 76 mm. Refractive index matching of the cladding to the core and core mode competition are introduced to extend the core layer diameter of the single-transverse-mode crystalline waveguide to 332 μm so that the large-size rectangular core crystalline waveguide can output the fundamental mode (relevant theoretical calculations are reported in Ref. [14]). The crystalline waveguide is wrapped in indium foil and clamped between two water-cooled copper blocks for efficient cooling, and maintained at 20 °C.

The cavity setup is shown in Fig. 3. A flat-flat cavity is used in the large-size rectangular core crystalline waveguide mode-locked laser, which is obtained by adding three sets of 4f systems in a flat-flat short cavity. A fixed proportion of the light field of the waveguide is transmitted to the SESAM, and the final cavity length is achieved without changing the Q parameter of a Gaussian beam [18]. The light spot size on the SESAM can be changed quantitatively by changing the focal length ratio of the last set of mirrors. Negative group-delay dispersion (GDD) is introduced by five GTI mirrors (Shanghai Institute of Optics and Fine Mechanics, Chinese Academy of Sciences), which generate a total GDD of $-23,500 \text{ fs}^2$ per round trip. A Brewster plate with a thickness of 3 mm is used in the cavity to enforce stable linear polarization and suppress the oscillation of the 1050 nm laser. The pump source is a fiber-coupled diode laser with a center wavelength of 940 nm and a maximum power of 160 W [core size: 105 μm , numerical aperture (NA): 0.22]. The end-pump configuration is used in the experiment. The coupler consists of two convex lenses with focal lengths of 20 mm and 60 mm, respectively, which constitute a beam-expanding collimation system and focus the pump beam into the waveguide core with a waist spot diameter of 315 μm . The absorption rate of the core layer is maximized when the position of the pump beam waist is 2 mm inside the core layer. The maximum output power

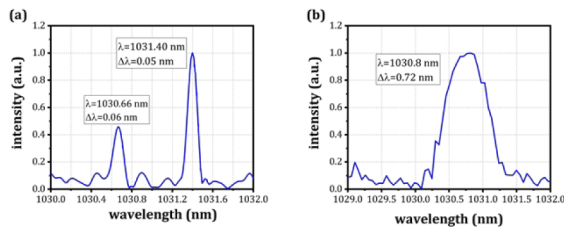


Fig. 4. Optical spectra of the large-size rectangular core crystalline waveguide mode-locking laser (a) without GTI mirrors and (b) after dispersion compensation.

is obtained when an output coupler with 50% transmittance at 1030 nm is used for continuous operation. The mode-locked laser uses an output coupler with a low transmittance ($T = 10\%$), which helps to improve the power density in the cavity.

Before mode-locking operation, the CW output of the cavity is measured. When the pump power is 160 W, the waveguide core absorbed pump power reaches 84 W, the pump absorption efficiency is 52.5% (the 45° dichromatic mirror presents a loss of 15% with a 940 nm laser), the output power is 21 W, and the optical-to-optical efficiency is 25%. Although the Yb:YAG crystals have a low doping concentration, the reabsorption phenomenon is still present and limits the optical-to-optical efficiency. The use of the double-clad crystal waveguide and the higher-power pump light effectively improve the optical-to-optical efficiency. We observe that two wavelengths, 1031 and 1050 nm, are obtained simultaneously. The CW signal detected by the oscilloscope is unstable due to a competitive relationship between these two wavelengths in a dynamic process. Inserting a polarizer into the cavity makes the laser work at 1031 nm. The spontaneous emission spectrum of the Yb:YAG crystal reveals that there are two main peaks under optical excitation [19]; the primary and secondary peaks are located at around 1030 nm and 1050 nm, respectively. One of the key issues for achieving different wavelength operation in a Yb:YAG laser is to precisely control the gain-to-loss ratios at 1030 nm and 1050 nm, and the corresponding polarization states of the two oscillations are slightly different.

During mode-locking operation, when the GTI mirrors are not used in the cavity, jitter is observed in the pulse signal. Two mode-locked pulse signals with slightly different central wavelengths are detected by a spectrometer. In Fig. 4(a), the two wavelengths are separated by 0.7 nm, which is different from the dual-wavelength phenomenon. This is spatial hole burning (SHB) [20]; because of this, Yb:YAG has a wide gain band and the crystal waveguide can support more than one longitudinal mode oscillation of different wavelengths in a standing wave cavity. When the GTI mirrors are added to the cavity, the spectrum of the output laser is broadened. As the spectral width is larger than 0.7 nm, the two main peaks can be covered. Figure 4(b) shows the spectral curve of continuous mode-locked output after dispersion compensation. The spectral width is broadened to 0.72 nm (full width at half maximum, FWHM) and the SHB is suppressed.

Figure 5 shows the output power curve during CWML operation. When the output power exceeds 2.85 W, the laser achieves stable CWML, and the experimental CWML threshold is close to the theoretically derived one. At the maximum pump power, the output mode-locking power is 16.9 W, and the pulsed incident on the SESAM is about 75 times the saturation fluence. In

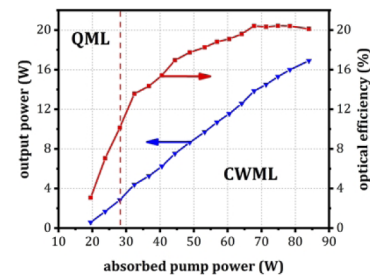


Fig. 5. Diagram of the relationship between output power and pump power during mode-locking operation.

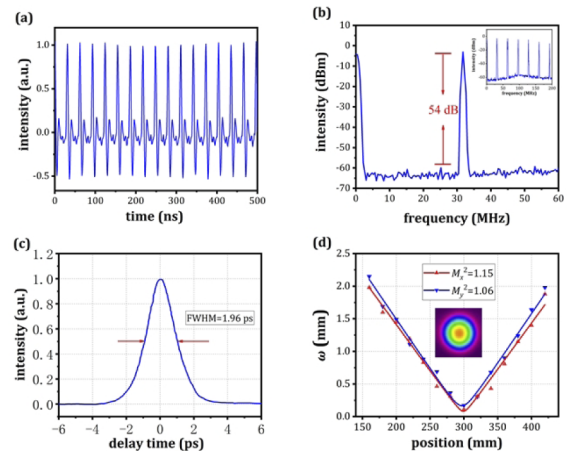


Fig. 6. Laser characteristics at the maximum output power. (a) Pulse train of CWML at the nanosecond time scale. (b) Radio-frequency spectrum (inset displays the spectrum recorded in a wide span of 200 MHz). (c) Autocorrelation trace. (d) Beam diameter versus the propagation distance of the output beam (inset displays the far-field beam spot measured by a CCD camera).

this regime, we observe no signs of damage, and the system can operate stably for a long time. The output power curve has no obvious saturation, and a higher laser output can be obtained by using a more powerful pump source.

Figure 6(a) shows the pulse signal that is detected by an oscilloscope. To claim the status of the mode-locking operation, the laser output pulses are monitored by a radio-frequency (RF) spectrum analyzer. As shown in Fig. 6(b), the measurement with a resolution bandwidth (RBW) of 100 kHz shows a clean peak at a fundamental repetition frequency of around 31.74 MHz. A high signal-to-noise ratio of 54 dB and the absence of side peaks confirm that excellent pulse-to-pulse stability is achieved without any evidence of Q-switching instabilities during mode locking. Figure 6(c) shows a single pulse shape (autocorrelation curve) and displays the autocorrelation trace with a FWHM of approximately 1.96 ps, corresponding to a time-bandwidth product of 0.39, slightly above the Fourier limit for a sech^2 pulse (0.315). This means that the pulse is weakly chirped. We acquired large-span microwave spectrum analyzer traces and scanned a long-range (200 ps) autocorrelator to confirm single-pulse operation.

The output beam quality is measured by the knife-edge method. A convex lens with a focal length of $f = 300$ mm is used to focus the output beam, and the focused beam spot diameter is measured at different positions using a beam-measuring

instrument. The fitting curve of the output beam is shown in Fig. 6(d). The beam quality M^2 in the x and y directions of the output beam are 1.15 and 1.06, respectively. It can be seen that the output beam quality in the x direction is notably worse than that in the y direction. This is because the heat dissipation effect on the upper and lower sides of the crystal heat sink is greater than that on the left and right sides. In addition, with a core size of 400 μm in the y direction, which exceeds the upper limit of the core size under the mode competition condition, the effect of the good output beam quality (1.06) is stronger than the effect of mode competition due to multiple oscillations. Although the cross section of the crystalline waveguide is rectangular, both the far-field spot of the output laser [inset of Fig. 6(d)] and the intracavity spot are nearly circular.

The next steps are to fabricate the large rectangular core crystal waveguide in a double-clad structure to improve the pump efficiency and to increase the output power by increasing the length of the crystal waveguide or connecting multiple crystal waveguides in series. Increasing the crystal length will accumulate more normal dispersion, and increasing the pulse peak power will enhance self-phase modulation (SPM). The mode-locking process relies on soliton pulse formation, which requires a balance between GDD and SPM, so how to compensate for the dispersion will be one of the problems that must be solved.

In conclusion, we have demonstrated the first mode-locked laser with a large-size rectangular core crystalline waveguide, to our knowledge. We succeeded in suppressing QML and SHB by using a cavity design and dispersion compensation, respectively. We obtained pulses as short as 1.96 ps with an average output power of 16.9 W at a repetition rate of 31.74 MHz. The expansibility of the power and the main problems were analyzed. It is expected that a mode-locked pulse laser with higher power will be obtained in future work.

Funding. Beijing Municipal Natural Science Foundation (4202007, KZ202110005010); National Natural Science Foundation of China (62075003).

Disclosures. The authors declare no conflicts of interest.

Data availability. No data were generated or analyzed in the presented research.

REFERENCES

1. A. Ancona, S. Doring, C. Jauregui, F. Roser, J. Limpert, S. Nolte, and A. Tunnermann, *Opt. Lett.* **34**, 3304 (2009).
2. A. Ozawa, Z. G. Zhao, M. Kuwata-Gonokami, and Y. Kobayashi, *Opt. Express* **23**, 15107 (2015).
3. M. Hentschel, R. Kienberger, C. Spielmann, G. A. Reider, N. Milosevic, T. Brabec, P. Corkum, U. Heinzmann, M. Drescher, and F. Krausz, *Nature* **414**, 509 (2001).
4. M. Maiuri, M. Garavelli, and G. Cerullo, *J. Am. Chem. Soc.* **142**, 3 (2020).
5. C. M. Caves, *Phys. Rev. D* **26**, 1817 (1982).
6. M. Hofer, M. E. Fermann, F. Haberl, M. H. Ober, and A. J. Schmidt, *Opt. Lett.* **16**, 502 (1991).
7. B. Ortac, O. Schmidt, T. Schreiber, J. Limpert, A. Tunnermann, and A. Hideur, *Opt. Express* **15**, 10725 (2007).
8. J. A. Der Au, G. J. Spuhler, T. Sudmeyer, R. Paschotta, R. Hovel, M. Moser, S. Erhard, M. Karszewski, A. Giesen, and U. Keller, *Opt. Lett.* **25**, 859 (2000).
9. J. E. Bernard and A. J. Alcock, *Opt. Lett.* **18**, 968 (1993).
10. U. Griebner and H. Schonhagel, *Opt. Lett.* **24**, 750 (1999).
11. D. P. Shepherd, A. Choudhary, A. A. Lagatsky, P. Kannan, S. J. Beecher, R. W. Eason, J. I. Mackenzie, X. Feng, W. Sibbett, and C. T. A. Brown, *IEEE J. Sel. Top. Quantum Electron.* **22**, 16 (2016).
12. S. Y. Choi, T. Calmano, F. Rotermund, and C. Kränkel, *Opt. Express* **26**, 5140 (2018).
13. X. Mu, S. Meissner, H. Meissner, and A. W. Yu, *Opt. Lett.* **39**, 6331 (2014).
14. X. Hu, D. J. Cheng, H. Lei, Y. L. Hui, M. H. Jiang, and Q. Li, *Opt. Lett.* **44**, 2685 (2019).
15. C. Honninger, R. Paschotta, F. Morier-Genoud, M. Moser, and U. Keller, *J. Opt. Soc. Am. B* **16**, 46 (1999).
16. T. Wu, Y. Hui, Z. Yan, Z. Li, and Q. Li, *Opt. Laser Technol.* **89**, 196 (2017).
17. Y. L. Hui, Q. Liu, X. Hu, Z. D. Zhu, H. Lei, and Q. Li, *Opt. Express* **29**, 2099 (2021).
18. S. V. Marchese, T. Sudmeyer, M. Golling, R. Grange, and U. Keller, *Opt. Lett.* **31**, 2728 (2006).
19. F. X. Kaertner, B. Braun, and U. Keller, *Appl. Phys. B* **61**, 569 (1995).
20. B. Braun, K. J. Weingarten, F. X. Kaertner, and U. Keller, *Appl. Phys. B* **61**, 429 (1995).